

Topology, noise, and parallel updates in circular opinion dynamics

Wioletta M. Ruszel¹ and Cristian Spitoni²

Mathematical Institute, Utrecht University, Utrecht, The Netherlands

Abstract. We study a circular opinion dynamics model with local mid-point interactions, extended to allow parallel updates of multiple sites. On a ring, the dynamics admits twisted states associated with integer winding numbers. We investigate how bi-modal noise, which drives opinions toward two antipodal directions, affects these configurations. Numerically, we find that noise both destabilizes winding states and induces a flip-flop regime, characterized by macroscopic switching between preferred orientations. We introduce order parameters that distinguish topological trapping from symmetry breaking, providing a simple macroscopic description of the dynamics.

1 Introduction

Opinion dynamics models provide a framework for understanding how simple, local interactions among agents give rise to complex collective behavior at the macroscopic scale ([5]). When opinions are represented as angles on the circle ([1]), the geometry of the state space introduces topological features absent in linear models. In particular, configurations on a ring may carry a nontrivial winding number, leading to coherent twisted profiles that delay convergence to consensus.

In a recent work [2] we introduced the ACCA midpoint dynamics, a circular analogue of local averaging in which neighboring agents move to the midpoint along the shortest arc of the circle. Although consensus is the only absorbing configuration on finite graphs, numerical evidence shows that the dynamics may remain trapped for very long times near twisted profiles associated with fixed winding numbers.

In the present paper we investigate how this trapping behavior is modified by stochastic perturbations. We consider a noisy extension of the ACCA dynamics in which opinions are occasionally pushed toward two antipodal directions. These bi-modal perturbations generate a new collective phenomenon: the system alternates between two coherent macroscopic orientations, producing long-lived *flip-flop* transitions ([3]).

In addition, we introduce a generalized version of the dynamics with *parallel updates*, in which multiple disjoint interactions and stochastic perturbations act

¹ w.m.ruszel@uu.nl

² c.spitoni@uu.nl

simultaneously on subsets of agents. This extension allows us to interpolate between asynchronous and partially synchronous regimes, and to investigate how the degree of parallelism affects the formation and stability of coherent structures.

Our aim is to characterize these regimes through suitable macroscopic observables. We introduce the models in Section 2 and the order parameters that distinguish winding trapping from antipodal switching in Section 3. They will be used in Section 4 in the simulations to study the interplay between topological constraints, midpoint averaging, bi-modal noise, and parallel updates. Finally, we discuss future developments in Section 5.

2 Model and notation

This section uses the notation introduced in [2]. We consider a system of N agents located on the vertices $V_N := \{1, \dots, N\}$ of a one-dimensional graph with edge set \mathcal{E} . Each agent carries an opinion represented by an angle on the circle, so that the configuration at time t is $\theta_t = (\theta_t(1), \dots, \theta_t(N)) \in \Omega_N := [-\pi, \pi)^N$. Throughout the paper angles are interpreted modulo 2π . For $x \in \mathbb{R}$, we define the *wrapped difference*

$$\text{wrap}_\pi(x) := x - 2\pi \left\lfloor \frac{x + \pi}{2\pi} \right\rfloor \in [-\pi, \pi). \quad (1)$$

For two opinions α, β we write $\text{wrap}_\pi(\beta - \alpha)$ for their shortest circular difference.

We consider two possible interaction graphs: the *path* with edge set $\mathcal{E}_\emptyset = \{(i, i+1) : 1 \leq i \leq N-1\}$, and the *ring* with periodic boundary conditions $\mathcal{E}_p = \{(i, i+1) : 1 \leq i \leq N-1\} \cup \{(N, 1)\}$. Hence, in this paper $\mathcal{E} \in \{\mathcal{E}_\emptyset, \mathcal{E}_p\}$. For an edge $e = (i, j)$ we define the *circular increment*

$$\delta_t(e) := \text{wrap}_\pi(\theta_t(j) - \theta_t(i)). \quad (2)$$

We define the winding number, which will be an integer on the ring, in the following way:

$$W_t := \frac{1}{2\pi} \sum_{e \in \mathcal{E}_p} \delta_t(e). \quad (3)$$

2.1 ACCA midpoint dynamics

We recall the ACCA (*Asynchronous Continuous-space Cellular Automaton*) midpoint rule introduced in [2]. At each discrete time step an edge is selected uniformly at random and the two corresponding opinions move to their circular midpoint along the shortest arc.

Algorithm 1 ACCA midpoint dynamics

- 1: Choose an edge $e = (i, j)$ uniformly at random from \mathcal{E}
 - 2: $\delta \leftarrow \text{wrap}_\pi(\theta_t(j) - \theta_t(i))$
 - 3: $\theta_{t+1}(i) \leftarrow \text{wrap}_\pi(\theta_t(i) + \delta/2)$
 - 4: $\theta_{t+1}(j) \leftarrow \text{wrap}_\pi(\theta_t(j) - \delta/2)$
 - 5: All other sites remain unchanged
-

Thus, the selected pair is replaced by its midpoint along the shortest arc of the circle. This local averaging mechanism decreases disagreement and drives the system toward consensus ([4]). We refer the interested reader to [2] for further properties of the dynamics.

2.2 ACCA dynamics with bi-modal noise

To investigate the robustness of the dynamics, we introduce a noisy variant in which opinions are occasionally perturbed toward two *antipodal* directions.

Algorithm 2 ACCA dynamics with bi-modal noise

- 1: Apply **Algorithm 1** to configuration θ_t and obtain the configuration θ_t^*
 - 2: Choose site $k \in V_N$ uniformly from $\{1, \dots, N\}$
 - 3: Choose $a \in \{0, \pi\}$ with probability 1/2
 - 4: $\theta_{t+1}(k) \leftarrow \text{wrap}_\pi(\theta_t^*(k) + \varepsilon \text{wrap}_\pi(a - \theta_t^*(k)))$
-

The perturbation moves the chosen opinion a fraction ε of the shortest circular distance toward the target angle a . For $\varepsilon = 0$ the dynamics reduces to the non-noisy ACCA model, while for $\varepsilon > 0$ the system experiences persistent symmetric forcing toward the two antipodal directions 0 and π (see Figure 1).

2.3 ACCA dynamics with parallel updates and bi-modal noise

We introduce a generalization of the ACCA dynamics in which both the local averaging mechanism and the stochastic perturbation act simultaneously on multiple sites. This variant interpolates between the original sequential dynamics and a more parallel, cellular-automaton-like regime, allowing one to investigate how collective updates affect the formation and stability of coherent structures.

At each time step, a collection of disjoint edges is selected and updated in parallel according to the midpoint rule, producing an intermediate configuration. A stochastic perturbation is then applied in parallel to a randomly chosen subset of sites. The sizes of these subsets are fixed parameters of the dynamics, controlling the degree of parallelism in the deterministic and stochastic components.

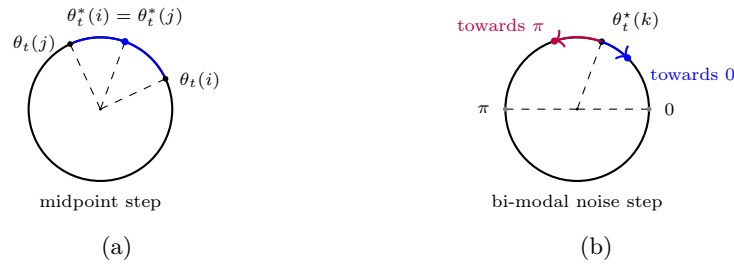


Fig. 1: One update of the ACCA dynamics under **Algorithm 2**. (a) A randomly chosen edge (i, j) is updated by the circular midpoint rule, producing an intermediate state θ_t^* . (b) Then a site k is selected uniformly and its opinion is moved a fraction ε toward one of the two antipodal targets $a \in \{0, \pi\}$, each chosen with probability $1/2$. In the schematic, the displacement is shown with $\varepsilon = 0.35$ for visibility.

Algorithm 3 ACCA dynamics with parallel updates and bi-modal noise

- 1: Fix integers $k_{\text{mid}} \geq 1$ and $k_{\text{noise}} \geq 0$
 - 2: Sample a set $\mathcal{F} \subseteq \mathcal{E}$ with $|\mathcal{F}| = k_{\text{mid}}$ of disjoint edges uniformly at random
 - 3: Set $\theta_t^* \leftarrow \theta_t$
 - 4: **for** each edge $(i, j) \in \mathcal{F}$ **do**
 - 5: apply **Algorithm 1**, obtaining $\theta_t^*(i), \theta_t^*(j)$
 - 6: **end for**
 - 7: Sample a subset $B \subseteq V_N$ with $|B| = k_{\text{noise}}$ uniformly at random
 - 8: Set $\theta_{t+1} \leftarrow \theta_t^*$
 - 9: **for** each $i \in B$ **do**
 - 10: apply **Algorithm 2**, obtaining $\theta_{t+1}(i)$
 - 11: **end for**
-

In this formulation, the midpoint interaction is applied simultaneously to a collection of k_{mid} disjoint edges. The disjointness condition ensures that each site is involved in at most one update, so that the parallel step is well defined. All midpoint moves are computed from the same configuration θ_t , yielding an intermediate state θ_t^* .

Starting from this intermediate configuration, a stochastic perturbation is applied in parallel to a subset B of k_{noise} sites, chosen uniformly without replacement. Each selected site is updated independently: a target angle $a \in \{0, \pi\}$ is drawn with probability $1/2$, and the opinion is moved a fraction ε of the shortest circular distance towards this target. Sites not in B remain unchanged.

For $k_{\text{mid}} = 1$ and $k_{\text{noise}} = 1$, the dynamics reduces to the standard sequential ACCA model with bi-modal noise defined in **Algorithm 2**. Increasing k_{mid} enhances the degree of parallel local averaging, while increasing k_{noise} produces more spatially extended and independent stochastic perturbations, which allows to interpolate between asynchronous and partially synchronous regimes.

2.4 Properties of ACCA midpoint dynamics

The qualitative behavior of the ACCA midpoint dynamics is well understood (see [2]). On finite connected graphs with open boundary conditions the system converges almost surely to consensus, as proved for related midpoint models in [4] and for the ACCA dynamics in our previous work ([2]).

Under periodic boundary conditions the situation is different. Because of the circular geometry, configurations can organize into metastable (trapped) twisted profiles characterized by a non-zero winding number W_t . In such states the opinions form an approximately linear phase profile along the ring. Although these configurations are not stationary, the midpoint averaging dynamics keeps the system close to the twisted manifold for very long times, producing a form of dynamical trapping.

When stochastic perturbations are introduced ($\varepsilon > 0$), the dynamics changes qualitatively. The bi-modal forcing toward the antipodal angles 0 and π gradually destabilizes the twisted profiles and may induce collective switching between preferred orientations. Numerical experiments reveal a characteristic *flip-flop* regime in which the macroscopic state alternates between two coherent orientations.

3 Order parameters

The coexistence of winding trapping and antipodal switching requires two distinct macroscopic diagnostics: one sensitive to topological structure and one sensitive to global orientation.

In order to detect the onset of consensus, we first recall known *order parameters*. Analogously to what is typically done for the Kuramoto model, as for example in [6], we can investigate the order parameters $R(t)$ and $\psi(t)$ defined as follows:

Definition 1 (Order parameters R and ψ). Let $\theta_t \in \Omega_N$ denote a configuration at time t . We then define the order parameters $R(t)$ and $\psi(t)$ by:

$$R(t)e^{i\psi(t)} := \frac{1}{N} \sum_{j=1}^N e^{i\theta_t(j)}. \quad (4)$$

The order parameter R quantifies the degree of alignment among opinions, while ψ represents the average opinion. Each opinion is represented as a direction and is represented as a point on the unit circle. By summing these directions as vectors, we obtain a resultant vector pointing in the average direction ψ , whose magnitude R indicates the strength of alignment. If $R = 0$, there is no alignment, i.e. the opinions are uniformly distributed around the circle. If $R = 1$ there is perfect consensus, which means that all opinions are identical. Thus, the closer R is to 1, the more synchronized the opinions are. In the noisy extension with symmetric bi-modal perturbations toward the two antipodal angles 0 and

π , the dynamics may display a *flip-flop regime*, in which the configuration alternates between two coherent macroscopic orientations. In this regime the system concentrates close to the two states

$$\theta_i \approx \frac{\pi}{2} \quad \text{or} \quad \theta_i \approx -\frac{\pi}{2}, \quad i = 1, \dots, N.$$

Such configurations are not well detected by the classical Kuramoto order parameter $R(t)$ alone, since $R(t)$ only measures the degree of alignment but not the orientation of the collective state. To distinguish the two branches it is convenient to consider the macroscopic projection onto the orthogonal axis,

$$Y(t) := \frac{1}{N} \sum_{j=1}^N \sin(\theta_t(j)). \quad (5)$$

Configurations concentrated near $\theta = \frac{\pi}{2}$ yield $Y(t) \approx 1$, while configurations concentrated near $\theta = -\frac{\pi}{2}$ give $Y(t) \approx -1$. Therefore the sign of $Y(t)$ distinguishes the two *flip-flop* orientations, and transitions of $Y(t)$ between positive and negative plateaus provide a clear macroscopic signature of the flip-flop dynamics.

In order to detect winding configurations we introduce an order parameter based on a nonparametric correlation coefficient on the torus, analogous to Kendall's τ (see [7]). This observable measures the statistical alignment between two angular variables while taking into account the periodic geometry.

Let $P_1 = (\theta_1, \phi_1)$ and $P_2 = (\theta_2, \phi_2)$ be two points on the torus. Intuitively, the pair is said to be *concordant* if the circular order from θ_1 to θ_2 and from ϕ_1 to ϕ_2 has the same orientation, and *discordant* otherwise.

Definition 2 (Weighted toroidal Kendall coefficient). *Let (Θ_1, Φ_1) and (Θ_2, Φ_2) be i.i.d. copies of (Θ, Φ) . The weighted toroidal Kendall coefficient is defined as:*

$$\tau_1 := \frac{\mathbb{E}[\text{wrap}_\pi(\Theta_2 - \Theta_1) \text{sign}(\text{wrap}_\pi(\Phi_2 - \Phi_1))]}{\mathbb{E}[|\text{wrap}_\pi(\Theta_2 - \Theta_1)|]}, \quad (6)$$

where it is assumed that the denominator is non-zero.

The normalization ensures that $\tau_1 \in [-1, 1]$. The coefficient τ_1 measures the correlation between the circular ordering of Θ and that of Φ , while preserving the magnitude of the wrapped difference.

We now compute τ_1 for an ideal twisted configuration. Consider the *winding configuration* on the ring

$$\Phi_i := \alpha + W \Theta_i \pmod{2\pi}, \quad W \in \mathbb{Z}, \quad \Theta_i \sim \text{Unif}(-\pi, \pi], \quad (7)$$

with $i \in \{1, 2\}$. We have the following theorem, whose proof is given in Appendix A:

Theorem 1. *Under the ideal winding configuration (7), for $W \neq 0$ one has*

$$\tau_1 = \frac{(-1)^{W+1}}{W}. \quad (8)$$

In particular $|\tau_1| = \frac{1}{|W|}$, for $W \neq 0$.

Thus the observable τ_1 detects twisted configurations through a characteristic inverse dependence on the winding number. Despite the classical Kuramoto order parameter $R(t)$ is well suited to detect convergence to global consensus, it does not distinguish between a flat profile and a coherent twisted configuration with nonzero winding number. In a trapping winding state the configuration is highly ordered along the ring but not phase-aligned, and therefore $R(t)$ may remain moderate even though the system is strongly structured.

4 Results

All the experiments in this section are started from a random configuration $\theta_0 \in \Omega_N$ with $\theta_0(i) \stackrel{i.i.d.}{\sim} \text{Unif}[-\pi, \pi]$, for $i \in V_N$, where $N = 100$.

Figure 2 illustrates the midpoint ACCA dynamics of **Algorithm 1** under periodic boundary conditions (i.e., $\mathcal{E} = \mathcal{E}_p$) for a configuration with winding number $W = 2$. In particular, in the panel (b) the space-time heatmap (top left) shows that the system rapidly organizes into a twisted configuration characterized by an approximately linear phase profile along the ring. The winding structure is clearly detected by the circular Kendall coefficient $\tau_1(t)$ (bottom right), which quickly converges to a constant value consistent with the theoretical prediction $|\tau_1| = 1/|W| = 1/2$. At the same time the classical Kuramoto order parameter $R(t)$ (top right) remains small, indicating that the configuration is highly ordered along the ring but not phase-aligned, as expected for a twisted state. Finally, the macroscopic orientation observable $Y(t)$ (bottom left) fluctuates around zero, which reflects the absence of a preferred global orientation in the deterministic twisted configuration. Together, these observables clearly distinguish winding trapping from global consensus and provide complementary diagnostics of the system's macroscopic organization.

Figure 3 illustrates the effect of bi-modal perturbations (i.e. **Algorithm 2**) under periodic boundary conditions. In contrast with the deterministic case, where the configuration remains trapped near a twisted ramp associated with a fixed winding number, the presence of noise progressively destabilizes this structure. For weak perturbations (e.g., $\varepsilon = 0.002$), the ramp remains clearly visible in the space-time heatmap and the configuration stays close to a coherent winding profile for long times. As the noise intensity increases (e.g., $\varepsilon = 0.02$), however, the ramp is gradually destroyed and the system no longer maintains a stable linear profile along the ring. The resulting dynamics is not characterized by well-formed plateaus around the two flip-flop states. Rather, the observable $Y(t)$ displays large collective fluctuations, indicating repeated global reorientations of the configuration. These fluctuations occasionally bring the system

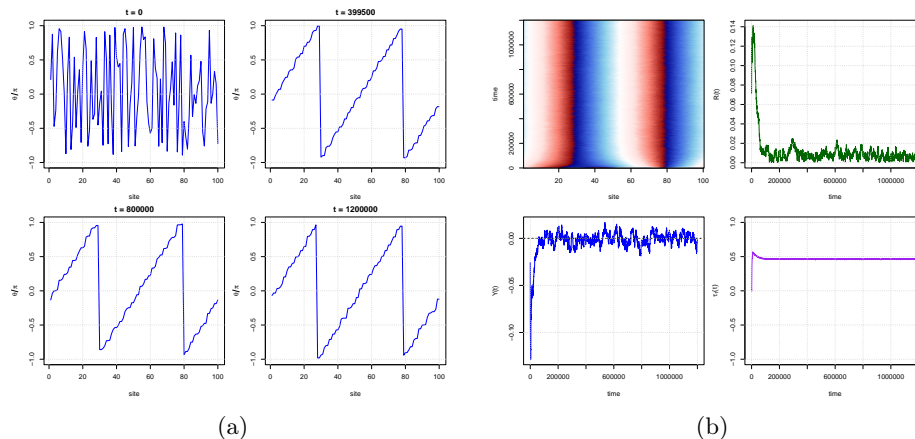


Fig. 2: ACCA dynamics with $N = 100$ and $\varepsilon = 0$ under periodic boundary conditions. (a) Configuration snapshots at four different times. (b) In the four panels are respectively plotted: the heatmap of the time evolution, the order parameters $R(t)$, $Y(t)$ and τ_1 as function of time

close to the two preferred orientations, but without producing the clear plateaus observed under open boundary conditions. At the same time, the classical Kuramoto order parameter $R(t)$ remains relatively small, showing that the system does not approach global consensus, while the toroidal Kendall coefficient $\tau_1(t)$ progressively departs from the deterministic value associated with the winding sector. This indicates that bi-modal perturbations gradually erode the topological trapping induced by the ACCA dynamics: the winding structure becomes less stable, and the evolution is increasingly dominated by large-scale fluctuations rather than by confinement near a coherent twisted ramp.

Figures 4–6 illustrate the dynamics under open boundary conditions (i.e., $\mathcal{E} = \mathcal{E}_\theta$). In the deterministic case ($\varepsilon = 0$), the system converges to consensus, as established in [4, 2]. The introduction of bi-modal perturbations leads to a qualitatively different regime. Even for very small noise intensity, the configuration rapidly organizes into states concentrated near the two antipodal orientations $\pm\pi/2$. This reflects the breaking of rotational symmetry induced by the bi-modal noise. The observable $Y(t)$ clearly captures this behavior: it alternates between positive and negative plateaus, corresponding to configurations concentrated near $\theta \approx \pi/2$ and $\theta \approx -\pi/2$. These plateaus indicate the presence of metastable macroscopic states. In contrast with the periodic case, no topological constraint is present, and the dynamics does not involve winding trapping. Instead, the behavior is dominated by the competition between midpoint averaging, which promotes local coherence, and bi-modal noise, which selects the two preferred orientations. As a result, the system repeatedly reorganizes around $\pm\pi/2$, producing a clear and robust flip–flop dynamics. Importantly, these states

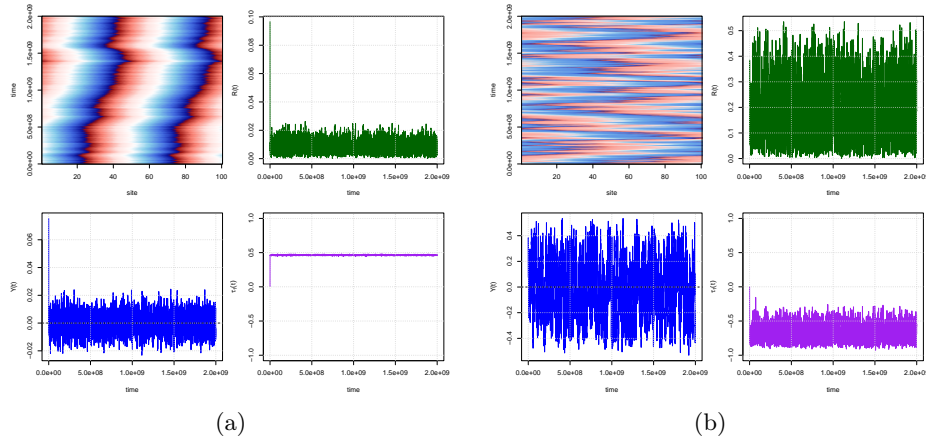


Fig. 3: Heatmap of the time evolution, the order parameters $R(t)$, $Y(t)$ and τ_1 as function of time for the ACCA dynamics with $N = 100$ and $\varepsilon \neq 0$ under periodic boundary conditions. (a) $\varepsilon = 0.002$; (b) $\varepsilon = 0.02$.

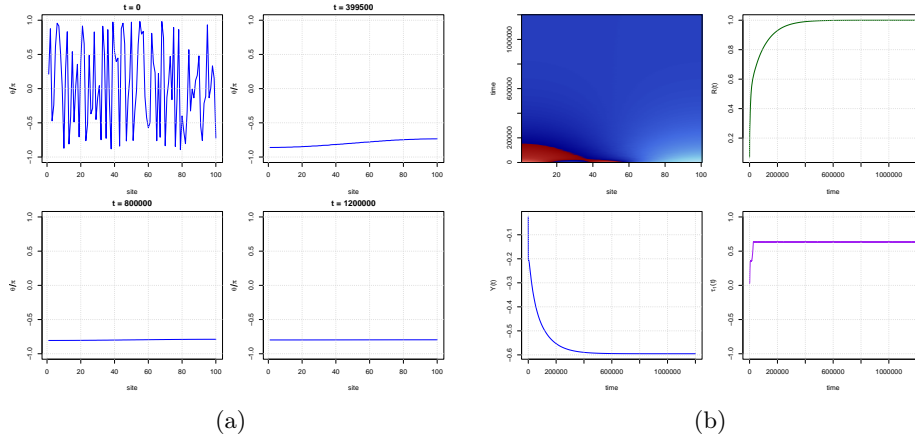


Fig. 4: ACCA dynamics with $N = 100$ and $\varepsilon = 0$ under open boundary conditions. (a) Configuration snapshots at four different times. (b) In the four panels are respectively plotted: the heatmap of the time evolution, the order parameters $R(t)$, $Y(t)$ and τ_1 as function of time

are not stationary: the configuration continues to evolve within each plateau, reflecting the persistent action of both averaging and noise.

We now investigate the generalized dynamics of **Algorithm 3** as a function of the burst parameters $k_{\text{mid}} \in \{1, 10, 20, 40\}$ and $k_{\text{noise}} \in \{0, 1, 10, 20, 40\}$, which control the degree of parallel midpoint averaging and the spatial extent of the stochastic perturbation. Figure 7 shows the late-time averages of the observables

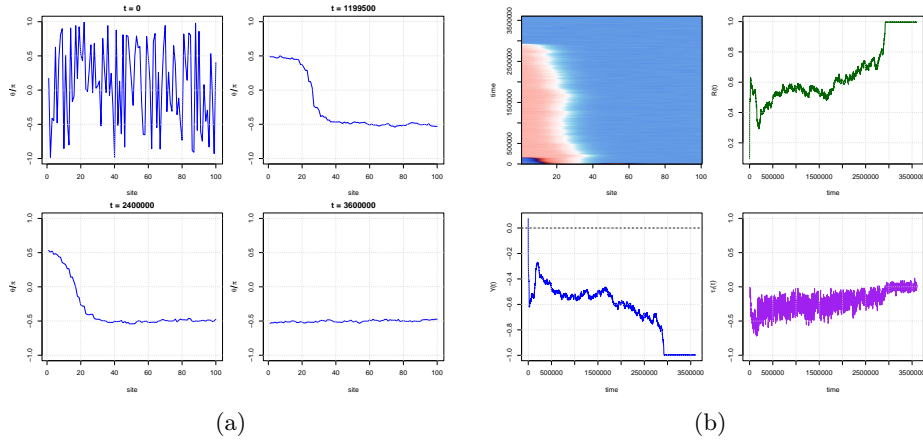


Fig. 5: ACCA dynamics with $N = 100$ and $\varepsilon = 0.002$ under open boundary conditions. (a) Configuration snapshots at four different times. (b) In the four panels are respectively plotted: the heatmap of the time evolution, the order parameters $R(t)$, $Y(t)$ and τ_1 as function of time

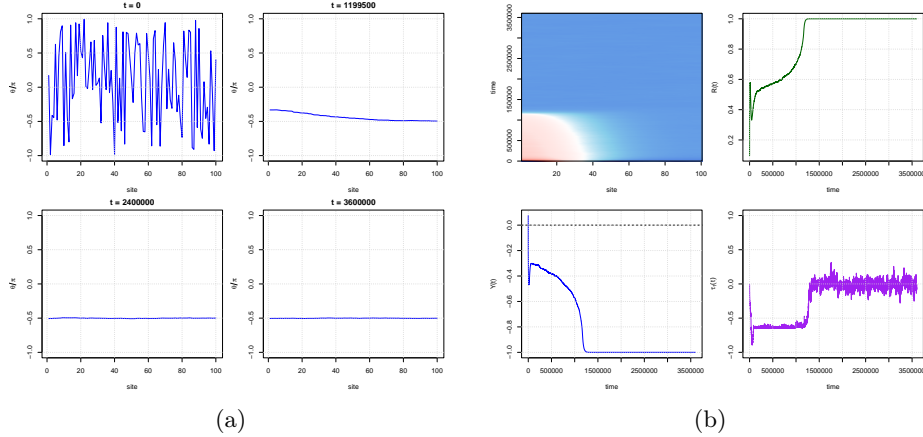


Fig. 6: ACCA dynamics with $N = 100$ and $\varepsilon = 0.0002$ under open boundary conditions. (a) Configuration snapshots at four different times. (b) In the four panels are respectively plotted: the heatmap of the time evolution, the order parameters $R(t)$, $Y(t)$ and τ_1 as function of time

R , $|Y|$, and $|\tau_1|$ as functions of $(k_{\text{mid}}, k_{\text{noise}})$. The two parameters play qualitatively different roles. Under open boundary conditions, increasing k_{mid} stabilizes the dynamics, while increasing k_{noise} destabilizes it. This is evident in panel (a), where larger k_{mid} leads to higher values of R , whereas larger k_{noise} suppresses alignment. Panel (b) shows that $|Y|$ behaves similarly: parallel midpoint up-

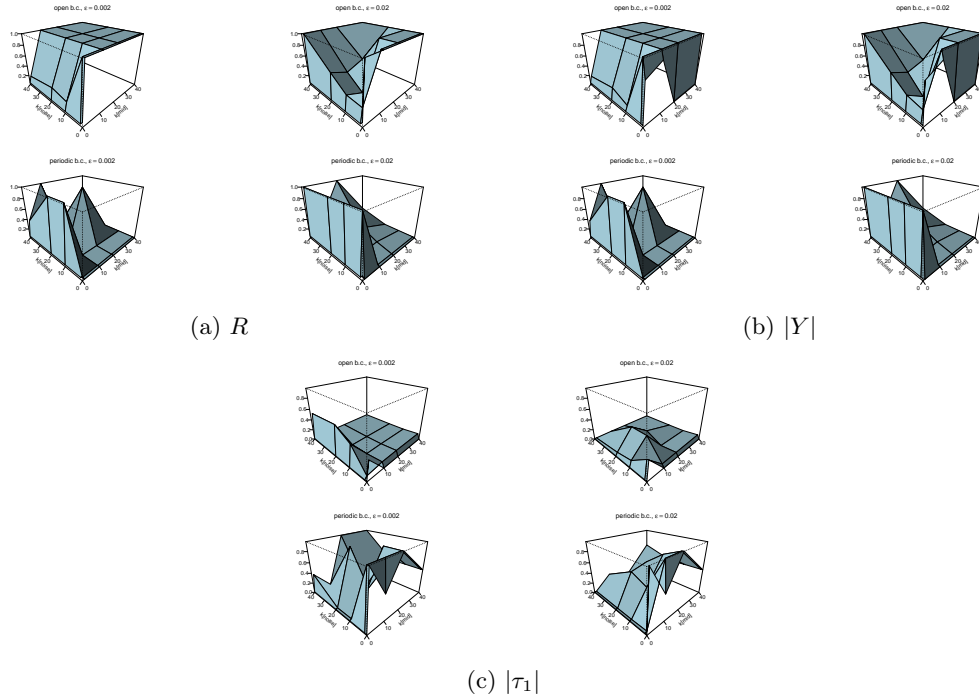


Fig. 7: Late-time values of R (panel (a)), $|Y|$ (panel (b)), and $|\tau_1|$ (panel (c)) for Algorithm 3 as functions of $(k_{\text{mid}}, k_{\text{noise}})$, under open and periodic boundary conditions ($N = 100$, $\varepsilon \in \{0.002, 0.02\}$). For clarity, the axes correspond to increasing values of k_{mid} and k_{noise} starting from the origin.

dates reinforce the selection of one of the two flip-flop branches, while spatially extended noise weakens this macroscopic orientation. Under periodic boundary conditions the behavior is more subtle. Panel (c) shows that the dependence of $|\tau_1|$ on k_{mid} is generally non-monotone. Parallel midpoint updates have a twofold effect: they smooth local fluctuations and can help maintain a coherent twisted profile, but when applied to many edges simultaneously they also induce more global rearrangements, which may destabilize a given winding sector. In contrast, increasing k_{noise} has a consistently destabilizing effect, as perturbations applied to many sites erode the topological trapping mechanism. Overall, the open system exhibits a largely monotone competition between stabilization and noise, whereas the periodic system shows a more intricate interplay between parallel averaging and winding preservation.

5 Discussion and future developments

The dynamics of the noisy ACCA model is governed by two distinct mechanisms. Under periodic boundary conditions, the winding number induces twisted config-

urations that confine the evolution near topological sectors, leading to trapping. Under open boundary conditions, this constraint is absent, and bi-modal noise drives the system toward two preferred orientations, producing a robust flip–flop regime.

Parallel burst updates clarify the interplay between these effects. Increasing the number of midpoint interactions enhances local averaging and stabilizes coherent structures, while increasing noisy updates destabilizes them. In open systems, these effects combine monotonically, whereas under periodic boundary conditions their interaction is non-monotone, reflecting the competition between averaging and topological constraints.

To summarize, the dynamics results from the interplay between local averaging, topology, and symmetry-breaking noise, which determines whether the system exhibits consensus, trapping, or persistent switching.

Future work includes quantifying transition times between winding sectors and studying structured or spatially correlated perturbations, bridging toward more realistic models of collective dynamics.

References

1. Acebrón, J.A., Bonilla, L.L., Vicente, C.J.P., Ritort, F., Spigler, R.: The Kuramoto model: A simple paradigm for synchronization phenomena. *Reviews of Modern Physics* **77**(1), 137–185 (2005). <https://doi.org/10.1103/RevModPhys.77.137>
2. Brockhaus, A., Ruszel, W.M., Spitoni, C.: Topological trapping in circular midpoint opinion dynamics. *ArXiv* (2026). <https://doi.org/10.48550/arXiv.2603.19774>
3. Collet, F., Ruszel, W.: Synchronization and spin-flop transitions for a mean-field XY model in random field. *Journal of Statistical Physics* **164**(3), 645–666 (2016)
4. Gantert, N., Heydenreich, M., Hirscher, T.: Strictly weak consensus in the uniform compass model on \mathbb{Z} . *Bernoulli* **26**(2), 1269–1293 (2020)
5. Lorenz, J.: Continuous opinion dynamics under bounded confidence: A survey. *International Journal of Modern Physics C* **18**(12), 1819–1838 (2007)
6. Strogatz, S.H.: From Kuramoto to Crawford: exploring the onset of synchronization in populations of coupled oscillators. *Physica D: Nonlinear Phenomena* **143**(1–4), 1–20 (2000). [https://doi.org/10.1016/S0167-2789\(00\)00094-4](https://doi.org/10.1016/S0167-2789(00)00094-4)
7. Zhan, X., Ma, T., Liu, S., Shimizu, K.: On circular correlation for data on the torus. *Statistical papers* **60**(6), 1827–1847 (2019)

A Proof of Theorem 1

Let

$$\tilde{\Delta} := \text{wrap}_\pi(\Theta_2 - \Theta_1).$$

Since Θ_1, Θ_2 are independent and uniformly distributed on $(-\pi, \pi]$, the wrapped difference $\tilde{\Delta}$ is uniformly distributed on $(-\pi, \pi]$. Indeed, if $X = \Theta_2 - \Theta_1$, the density of X is triangular on $(-2\pi, 2\pi)$:

$$f_X(x) = \frac{2\pi - |x|}{4\pi^2}.$$

Wrapping X into $(-\pi, \pi]$ folds the density onto this interval, and a direct computation shows that the resulting density is constant $1/(2\pi)$ (see proof Lemma 4.5 in [2]). Under the twisted assumption (7) we have $\text{wrap}_\pi(\Phi_2 - \Phi_1) = \text{wrap}_\pi(W\tilde{\Delta})$. Since $\tilde{\Delta}$ has a continuous distribution, the event $\tilde{\Delta} \in \pi\mathbb{Z}$ has probability zero. Moreover, $\text{wrap}_\pi(x) \in [-\pi, \pi)$, one has $\text{sign}(\text{wrap}_\pi(x)) = \text{sign}(\sin x)$ for all $x \notin \pi\mathbb{Z}$. Hence,

$$\text{sign}(\text{wrap}_\pi(\Phi_2 - \Phi_1)) = \text{sign}(\sin(W\tilde{\Delta})), \text{ a.s.}$$

Therefore

$$\mathbb{E}\left[\tilde{\Delta} \text{sign}(\text{wrap}_\pi(\Phi_2 - \Phi_1))\right] = \frac{1}{2\pi} \int_{-\pi}^{\pi} x \text{sign}(\sin(Wx)) dx. \quad (9)$$

Since the integrand is even, this becomes

$$\frac{1}{\pi} \int_0^{\pi} x \text{sign}(\sin(Wx)) dx.$$

On $(0, \pi)$ the function $\sin(Wx)$ changes sign at $x_k = k\pi/W$ for $k = 0, \dots, W$. Hence

$$\int_0^{\pi} x \text{sign}(\sin(Wx)) dx = \sum_{k=0}^{W-1} (-1)^k \int_{k\pi/W}^{(k+1)\pi/W} x dx.$$

A direct computation gives

$$\int_{k\pi/W}^{(k+1)\pi/W} x dx = \frac{(2k+1)\pi^2}{2W^2}.$$

Thus

$$\int_0^{\pi} x \text{sign}(\sin(Wx)) dx = \frac{\pi^2}{2W^2} \sum_{k=0}^{W-1} (-1)^k (2k+1).$$

The alternating sum evaluates to

$$\sum_{k=0}^{W-1} (-1)^k (2k+1) = (-1)^{W+1} W.$$

Hence

$$\mathbb{E}\left[\tilde{\Delta} \text{sign}(\text{wrap}_\pi(\Phi_2 - \Phi_1))\right] = \frac{(-1)^{W+1}\pi}{2W}.$$

Finally,

$$\mathbb{E}[|\tilde{\Delta}|] = \frac{1}{2\pi} \int_{-\pi}^{\pi} |x| dx = \frac{\pi}{2},$$

so that: $\tau_1 = \frac{(-1)^{W+1}}{W}$.